Designing water splitting catalysts using rules of thumb: advantages, dangers and alternatives

Oriol Piqué, Francesc Illas and Federico Calle-Vallejo*

Departament de Ciència de Materials i Química Física & Institut de Química Teòrica i Computacional (IQTCUB), Universitat de Barcelona, Martí i Franqués 1, 08028 Barcelona, Spain.

* Address correspondence to: f.calle.vallejo@ub.edu

Abstract

Thermodynamic analysis of the oxygen evolution reaction (OER) hints toward an intrinsic overpotential caused by the nonoptimal adsorption-energy scaling relation between OH and OOH. Consequently, nowadays it is a widely accepted yet unverified rule of thumb that breaking such scaling relation results in enhanced catalytic activity. In this Perspective, we show that breaking the OH-OOH scaling relation does not per se lower the OER overpotential. Instead, electrocatalytic symmetry and ease of optimization are shown to be key factors when screening for enhanced OER catalysts. The essence of electrocatalytic symmetry is captured by a descriptor called electrochemical-step symmetry index (ESSI). In turn, the ease of optimization and whether it should be scaling-based or scaling-free is provided by a procedure called δ–ε optimization. Finally, taking the search for bifunctional catalysts for oxygen electrocatalysis as an example, we show that the alternative analysis can be straightforwardly extended to other electrocatalytic reactions.

Table of contents entry

Breaking the OH-OOH scaling relation does not necessarily enhance water splitting electrocatalysis. Seeking “electrocatalytic symmetry” is a suitable alternative.

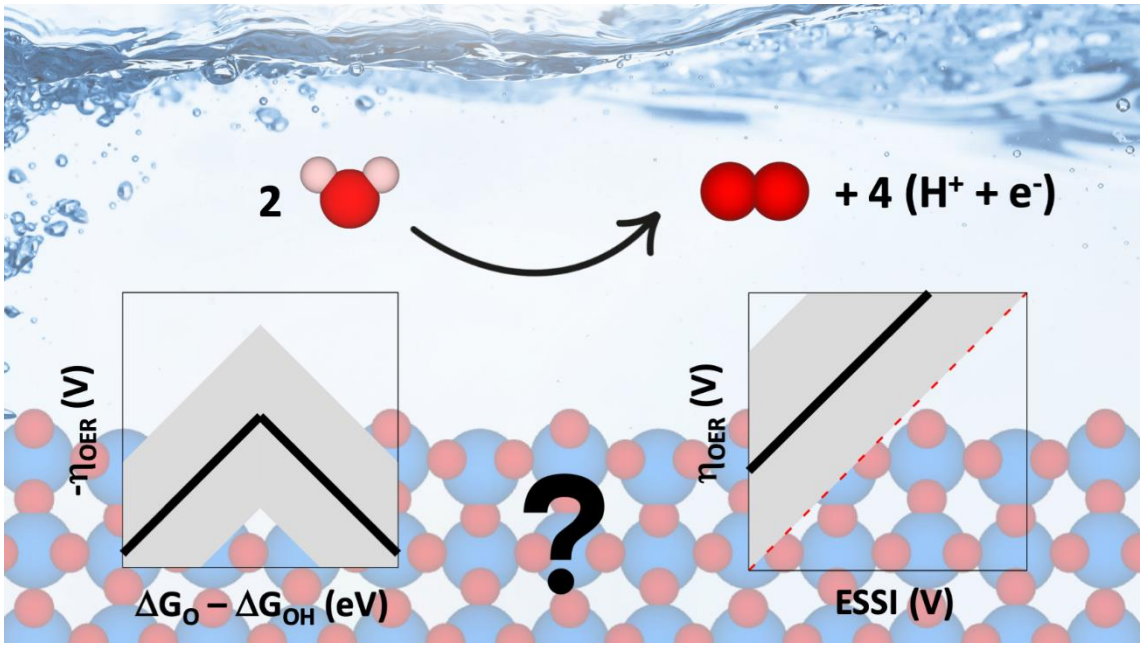

Introduction

It is a well-known experimental fact that the oxygen evolution reaction (OER: $2H_2O \rightarrow O_2 + 4H^+ + 4e^-$) at the anode of proton-exchange membrane electrolyzers is sluggish.[1,2] This, in addition to the scarceness, unsatisfactory durability and high prices of the most active electrocatalysts (usually Ir- or Ru-based) have prevented the extensive use of such electrolyzers for the generation of hydrogen.[3] While remarkable efforts have been made by experimenters to find new water-splitting catalysts[4,5] and other routes exist to split water (via photocatalysis, for instance),[6,7] the subject of this Perspective is the computational modelling of the electrochemical OER and how it is currently dominated by an uncertain rule of thumb.

Before we write and discuss such rule of thumb in detail, it is advisable to present the thermodynamic framework it is based on. First, the energetics of proton-electron pairs are described using the computational hydrogen electrode,[8] and it is assumed that all catalysts follow the same mechanistic pathway from H_2O to O_2:[9,10]

$$* + H_2O \rightarrow *OH + H^+ + e^- \quad (1)$$

$$*OH \rightarrow *O + H^+ + e^- \quad (2)$$

$$*O + H_2O \rightarrow *OOH + H^+ + e^- \quad (3)$$

$$*OOH \rightarrow * + O_2 + H^+ + e^- \quad (4)$$

There are three adsorbed intermediates in the mechanism, namely *O, *OH, and *OOH, so that the free energies of reaction (hereafter, referred to simply as energies) can be written as a function of those:

$$\Delta G_1 = \Delta G_{OH} \quad (5)$$

$$\Delta G_2 = \Delta G_O - \Delta G_{OH} \quad (6)$$

$$\Delta G_3 = \Delta G_{OOH} - \Delta G_O \quad (7)$$

$$\Delta G_4 = \Delta G_{O_2} - \Delta G_{OOH} \quad (8)$$

where $\Delta G_{O_2} = 4.92$ eV corresponds to the sum of Eqs. 5-8, and is equivalent to the equilibrium potential ($E^0 = 1.23$ V) multiplied by the total number of transferred electrons per catalytic cycle ($1.23\ \text{V} \times 4\text{e}^- = 4.92$ eV). Linear relations exist between the adsorption energies of those three intermediates on a wide variety of materials,[11-15] such that all reaction energies in Equations 5-8 can be written in terms of one of the three adsorption energies (either ΔG_O, ΔG_{OH}, or ΔG_{OOH}) or a linear combination of them (e.g. $\Delta G_O - \Delta G_{OH}$). In this model, the overpotential (in V) is determined by the largest positive reaction energy (in eV) in Equations 5-8:[9,10] $\eta_{OER} = \max\left(\{\Delta G_i\}\right)/e^- - 1.23$, with i = 1,2,3,4. The electrochemical step with such energy is deemed the potential-limiting step, which is different from the rate-determining step.[16] To conclude this section, note that within this model a catalyst with all $\Delta G_i = 1.23$ eV has null OER overpotential.

1. The upsides and downsides of adsorption-energy scaling relations

When aiming at understanding a physical and/or chemical phenomenon, a low number of degrees of freedom is advantageous, as the resulting model is likely simple and depends on a small set of independent parameters. Nevertheless, once the phenomenon is understood and the model is used for optimization purposes, a low number of degrees of freedom is problematic. Essentially, the linear dependence between certain parameters may prevent full optimization. As shown in Figure 1, that is exactly what happens during the OER for ΔG_O, ΔG_{OH}, and ΔG_{OOH}. The figure contains theoretical data collected from the literature for 155 different compounds belonging to different families, including

various types of oxides, porphyrins and functionalized graphitic materials.[10,17-25] We note that other families of compounds, such as chalcogenides and nitrides[26,27] might as well be included in the plot and in the analysis shown in the final parts of this article. The mean absolute error (MAE) between the linear fit and the calculated data points is only 0.17 eV for ΔG_{OOH} vs ΔG_{OH}, and 0.50 eV for ΔG_{O} vs ΔG_{OH}.

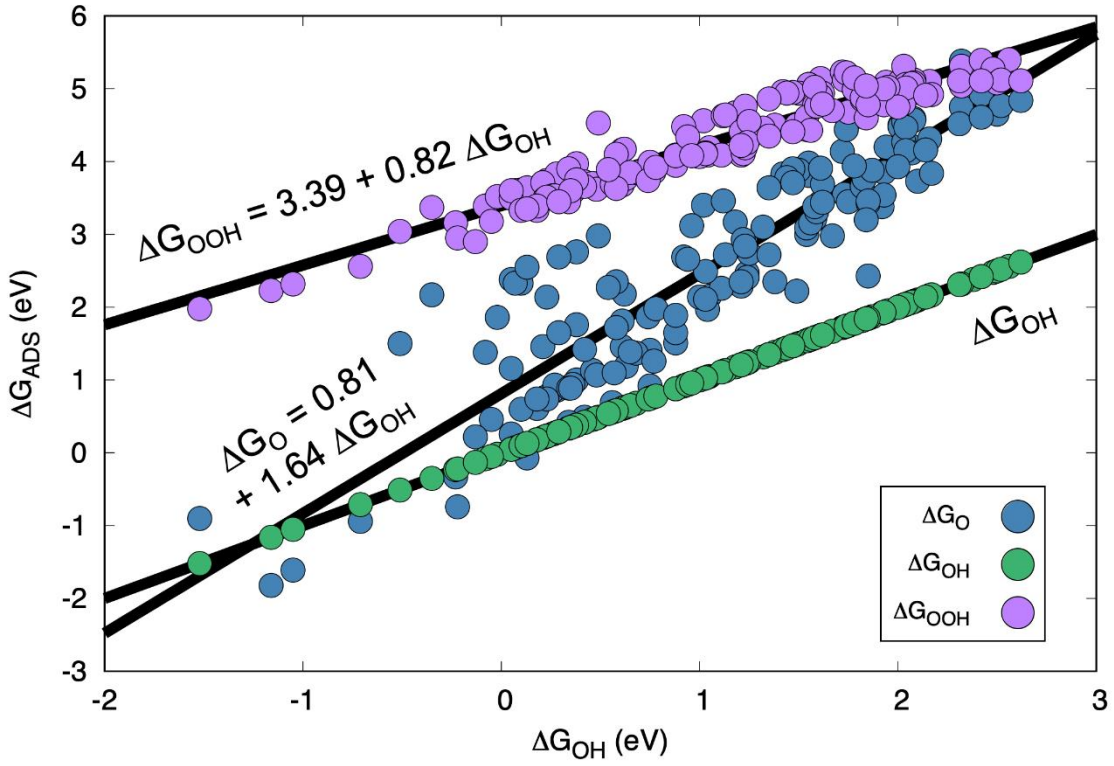

Figure 1. Adsorption-energy scaling relations between *O, *OH and *OOH. The data were taken from references 10,17-25. Least-squares linear fits are provided together with their corresponding equations. All the data in the figure are tabulated in the ESI.

Ideally, all reaction steps should consume 1.23 eV for the overpotential to be null, but adsorption-energy scaling relations seem to forbid it. This was first proposed in

2011,[10,28] after it was noted that the scaling relation between *OH and *OOH has a near unity slope and an intercept of ~3.2 ± 0.2 eV (see Figure S1).[10,17-25]

The consequences of such constant separation are far-reaching. To illustrate the matter, consider the sum of Equations 2 and 3, and the corresponding sum of reaction energies in Equations 6 and 7:

$$*OH + H_2O \rightarrow *OOH + 2H^+ + 2e^- \quad (9)$$

$$\Delta G_{2+3} = \Delta G_{OOH} - \Delta G_{OH} \quad (10)$$

For an ideal catalyst, ΔG_{2+3} should be $1.23\ \mathrm{V} \times 2\mathrm{e}^- = 2.46\ \mathrm{eV}$, given that all the steps involved are energetically identical. However, for a wide collection of catalysts it is usually in the range of 3.2 ± 0.2 eV, [10,17-25] see Figure S2. This, in addition to the fact that the overpotential is normally determined by steps 2 or 3, led to the conclusion that there exists an intrinsic OER overpotential due to scaling relations. Such overpotential can be calculated as: $\eta_{OER}^{SR} = (3.2 - 2.46)\mathrm{eV}/2e^- = 0.37\ \mathrm{V}$, where SR stands for scaling relations. In other words, the top of the so-called volcano plot is not located at 1.23 V but rather at 1.60 V. Note that a similar analysis holds, in principle, for the oxygen reduction reaction (ORR: $O_2 + 4H^+ + 4e^- \rightarrow 2H_2O$), where the top of the volcano is located at 0.86 V instead of 1.23 V.[17,29]

2. A simple rule of thumb for OER electrocatalysis

If there is an overpotential attributable to the OOH vs OH scaling, it is natural to hypothesize that its breaking will lead to enhanced OER electrocatalysis. The recipe is then to stabilize *OOH with respect to *OH.[10,30] This plausible yet unverified hypothesis

quickly became a pervasive rule of thumb for the design of new OER electrocatalysts and the concept was extended to other electrocatalytic reactions.[31-34]

The hypothesis was put to the test recently by plotting the calculated overpotential as a function of $\gamma_{OOH/OH}$ (in V), which is a metric for the degree of breaking of the OOH vs OH scaling relation ($\gamma_{OOH/OH} = \left(\Delta G_{OOH} - \Delta G_{OH} - 2.46\right)\text{eV}/2e^-$). As $\gamma_{OOH/OH}$ tends to zero, catalysts depart more and more from the scaling relation, which should correspond to a proportional lowering of the calculated OER overpotential. Unfortunately, as shown in Figure 2, this is not the case for a great variety of catalysts compiled from the literature.

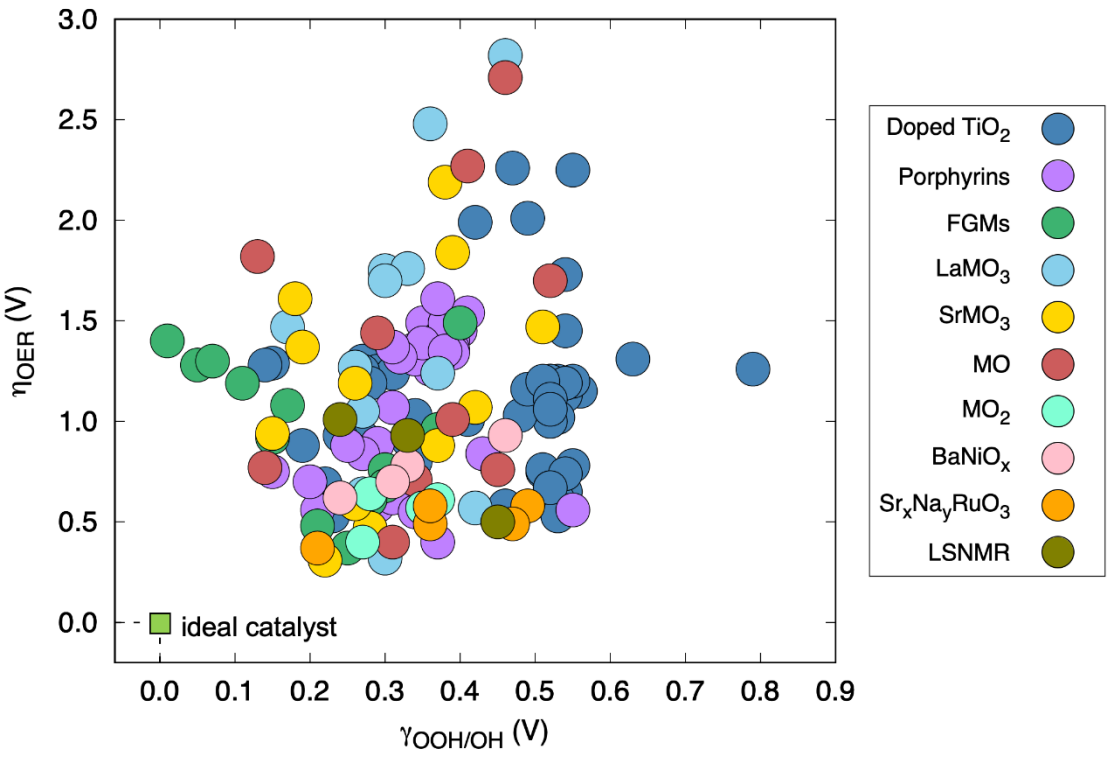

Figure 2. Calculated oxygen evolution overpotentials (η_{OER}) as a function of $\gamma_{OOH/OH}$, which is a metric for the degree of breaking of the OOH vs OH scaling relation ($\gamma_{OOH/OH} = \left(\Delta G_{OOH} - \Delta G_{OH} - 2.46\right)\text{eV}/2e^-$). The ideal catalyst is provided for comparison. The data were taken from references 10,17-25. All the data in the figure are tabulated in the ESI.

Given that a series of reasonable arguments led us to a visibly incorrect guess, namely that breaking scaling relations implies catalytic enhancement, it is worth finding the weak points in the analysis. One of them is the assumption of a sole reaction pathway for all materials. This is debatable but necessary to build an affordable framework wherein all catalysts can be directly compared. Nonetheless, we note that several alternative pathways have been proposed in the literature,[30,35-37] and that recent studies have shown that scaling relations can also be used to study competing pathways.[38] The structure- and composition-sensitive effects of solvation[20,39-41] are also worth incorporating in the model to improve its predictions, as *O, *OH, and *OOH are differently solvated depending on the material. Furthermore, if the potential- and rate-limiting steps of the reaction are different, the model might as well be misleading, as pointed out before.[16] Other modelling approaches also exist including reaction kinetics,[42,43] and recent works have been devoted to finding a unifying approach that accounts for OER thermodynamics and kinetics.[44,45]

Another weak point is the idea that stabilizing *OOH with respect to *OH indefectibly reduces η_{OER}. Looking at Equations 1-4, we conclude that this is only true for materials in which step 3 ($*O + H_2O \rightarrow *OOH + H^+ + e^-$) is potential limiting. From the 155 compounds considered here, only 45% of them belong to this group.

There is no effect on materials where the first ($* + H_2O \rightarrow *OH + H^+ + e^-$) and second ($*OH \rightarrow *O + H^+ + e^-$) steps are potential-limiting because *OOH is not involved in those.[46,47] Among all materials considered, 12 and 43% are respectively limited by steps 1 or 2.

Strikingly, if step 4 ($*OOH \rightarrow * + O_2 + H^+ + e^-$) is potential-limiting, stabilizing *OOH increases η_{OER} instead of decreasing it.[46,47] Although less than 1% of the materials

considered in this work are limited by this step, it usually limits the ORR on numerous materials.[47]

Therefore, the problem with the OOH-OH rule of thumb is that in at least 55% of the inspected cases it will likely have no effect on the overpotential or even increase it. Based on this, our conclusion is that one should probably focus on the actual potential-limiting step of the OER, which depends on every material, instead of trying to stabilize *OOH by default. The latter optimizes the sum of steps 2 and 3, which does not unambiguously result in a lowering of the calculated overpotential.

3. Electrocatalytic symmetry and a metric for it

As the OOH-OH rule of thumb is likely to fail in more than half of the cases, it is pertinent to ask if there are simple alternatives to evaluate and predict enhanced OER catalysts. As said before, the ideal catalyst has all $\Delta G_i = 1.23$ eV, which implies that it indeed breaks the OOH vs OH scaling relation and has null OER overpotential. Thus, at least from a thermodynamic point of view, it is reasonable to claim that the goal is for a catalyst to resemble as much as possible the ideal one. To quantitatively assess such resemblance, the electrochemical-step symmetry index (ESSI) was proposed:

$$ESSI = \frac{1}{n}\sum_{1}^{n}\left(\frac{\Delta G_i^{+}}{e^{-}} - E^{0}\right) \tag{11}$$

where ΔG_i^{+} corresponds to the reaction energies in Equations 1-4 that are larger than 1.23 eV, as only those can be potential-limiting, and E^{0} is the equilibrium potential (1.23 V). Examples of the assessment of ESSI can be found elsewhere.[22,23,24,46,47]

The correlation between ESSI, which is a metric for electrocatalytic symmetry, and OER overpotentials is apparent in Figure 3. In the analyzed set of 155 materials, the

mean absolute error (MAE) for the prediction of η_{OER} is 0.20 V and the maximum absolute error (MAX) is 0.69 V. For comparison, a linear fit of the data in Figure 2 provides a mean absolute error (MAE) of 0.38 V and a maximum absolute error (MAX) of 1.69 V. Besides, in Figure 4 we observe that the linear combination of $\gamma_{OOH/OH}$ and ESSI essentially follows the trends dictated by ESSI, and there are no substantial improvements in the MAE or the MAX (0.19 and 0.68 V, respectively).

To close this section, we note that, as ESSI is an average, it can be accompanied by error bars showing the dispersion of the data. In principle, catalysts with wide bars are easier to optimize than those with narrow bars.[46,47] Besides, ESSI can be calculated regardless of the presence or absence of scaling relations between reaction intermediates.

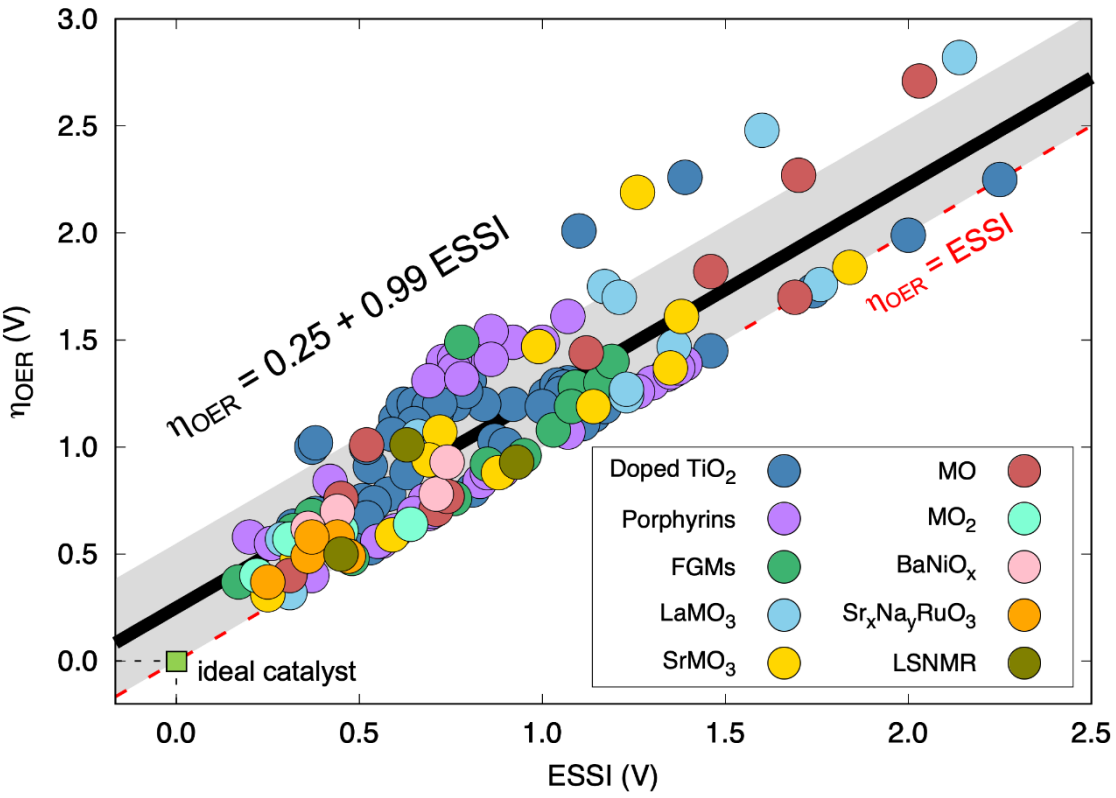

Figure 3. Calculated oxygen evolution overpotentials (η_{OER}) as a function of the electrochemical-step symmetry index (ESSI), which quantifies the resemblance of catalysts to the ideal one. The data were taken from references 10,17-25. All the data in the figure are tabulated in the ESI.

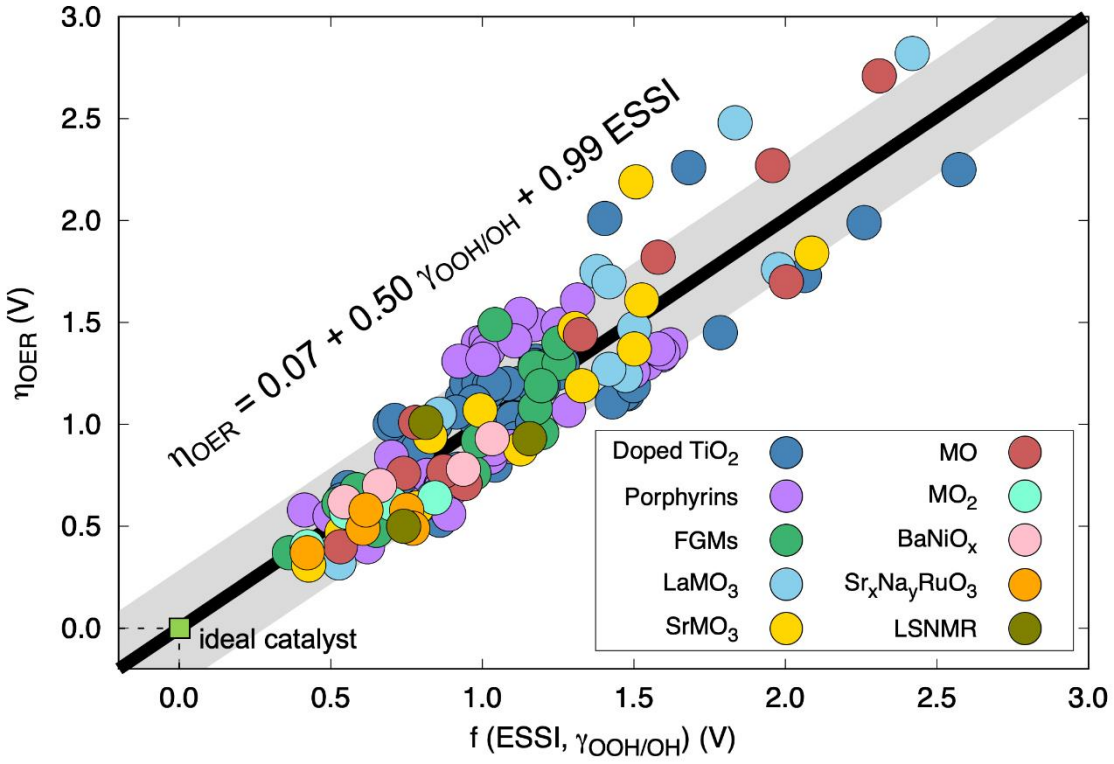

Figure 4. Calculated oxygen evolution overpotentials (η_{OER}) as a function of the electrochemical-step symmetry index (ESSI), which quantifies the resemblance of catalysts to the ideal one. The data were taken from references 10,17-25. All the data in the figure are tabulated in the ESI.

4. Quantitative prediction of catalytic enhancement

It is a common practice in experimental electrocatalysis to initially find a prospect material and subsequently engineer its structural and/or electronic properties to make it more active.[2,4] Intuitively, as a material approaches the top of the volcano plot, it gets progressively more difficult to further optimize it. However, how much a given material can be optimized is usually difficult to assess, so that the optimization of some may be slow and take many years.

A computational assessment of a given material's ease of improvement is provided by δ–ε optimization.[46] The procedure is simple and requires only the addition

of two parameters in Equations 5-8: δ, which is scaling-dependent; and ε, which is scaling free, as shown in Equations 12-15. Both parameters in Equations 12-15 are in the same units as the adsorption energies.

$$\Delta G_1 = \Delta G_{OH} + \delta \tag{12}$$

$$\Delta G_2 = \Delta G_O - \Delta G_{OH} + \delta \tag{13}$$

$$\Delta G_3 = \Delta G_{OOH} - \Delta G_O - \delta + \varepsilon \tag{14}$$

$$\Delta G_4 = \Delta G_{O_2} - \Delta G_{OOH} - \delta - \varepsilon \tag{15}$$

As it is the case for Equations 5-8, the sum of Equations 12-15 is $\Delta G_{O_2} = 4.92$ eV , as required by the energy conservation principle applied over the catalytic cycle in Equations 1-4. Since ε is scaling-free, it only affects *OOH. Conversely, δ is scaling-dependent, so it proportionally affects *O, *OH and *OOH. Accordingly, if ΔG_{OH} is modified by δ, then ΔG_{OOH} is also modified by δ and ΔG_O is modified by 2δ, which is justified by the slopes of the scaling relations in Figure 1. A positive value of δ causes a weakening of the adsorption energies, while a negative value of δ and ε causes their strengthening. Conservative ranges for δ and ε are [-0.3, 0.3] and [-0.3, 0] eV, respectively.[46] These imply that δ can either be a scaling-based destabilization or stabilization (via e.g. strain or geometric effects), while ε is a stabilization of *OOH (via tethering, nanoconfinement, ligand-adsorbate interactions).[30,46]

To illustrate the aim of δ–ε optimization, let us consider three materials: $Sr_{1-x}Na_xRuO_3$, $LaNiO_3$, and Ru FGM.[10,18,19,23,25] Their adsorption energies, reaction energies and calculated overpotentials before and after δ, ε and δ–ε optimization are shown in Table 1. We note that, although initially the OER overpotential of $LaNiO_3$ is lower than

that of $Sr_{1-x}Na_xRuO_3$ (0.37 vs 0.32 V), the latter is considerably easier to optimize. Indeed, upon δ optimization $LaNiO_3$'s overpotential decreases by 0.01 V, whereas that of $Sr_{1-x}Na_xRuO_3$ decreases by 0.17 V (0.31 vs 0.21 V). Interestingly, in none of the two perovskites was ε optimization leading to lower OER overpotentials (thus, ε = 0 eV), which stems from the two unoptimized materials being limited by the second electrochemical step ($*OH \rightarrow *O + H^+ + e^-$), in which *OOH is not involved.

The results for Ru FGM in Table 1 show that it benefits from δ, ε, and δ–ε optimizations. Separately, δ and ε optimizations lower the overpotential from 0.68 to 0.38 V, while their combination achieves 0.21 V. However, the difficulties for the experimental implementation of such optimizations likely increase from δ to ε to δ–ε, so that the former strategy is to be preferred over the latter two. Before closing this section, we emphasize that ESSI and δ–ε optimization can be used in conjunction, as recently shown in reference 46.

Table 1. Illustration of δ−ε optimization for $Sr_{1-x}Na_xRuO_3$,[23] $LaNiO_3$[21] and functionalized graphitic materials with RuN_4 sites (Ru FGM).[18,19] The two perovskites do not benefit from ε optimization. The values of δ and ε are provided in each case. In bold we marked the potential-limiting steps for every material. The free energies are in eV and the overpotentials in V.

compound	ΔG_O	ΔG_{OH}	ΔG_{OOH}	ΔG_1	ΔG_2	ΔG_3	ΔG_4	η_{OER}
$Sr_{1-x}Na_xRuO_3$	3.16	1.56	4.43	1.56	**1.60**	1.27	0.49	0.37
$Sr_{1-x}Na_xRuO_3$, δ = -0.17 eV	2.84	1.40	4.27	1.40	**1.44**	**1.44**	0.66	0.21
$LaNiO_3$	3.09	1.54	4.61	1.54	**1.55**	1.52	0.31	0.32
$LaNiO_3$, δ = -0.02 eV	3.05	1.52	4.59	1.53	**1.54**	**1.54**	0.32	0.31
Ru FGM	1.72	0.58	3.63	0.58	1.14	**1.91**	1.29	0.68
Ru FGM, δ = 0.30 eV	2.32	0.88	3.93	0.88	1.44	**1.61**	0.99	0.38
Ru FGM, ε = -0.30 eV	1.72	0.58	3.33	0.58	1.14	**1.61**	1.59	0.38
Ru FGM, δ = 0.30 eV, ε = -0.17 eV	2.32	0.88	3.76	0.88	**1.44**	**1.44**	1.16	0.21

5. Extension to other electrocatalytic reactions

The ESSI analysis and δ−ε optimization are not exclusively applicable to the OER but rather to all electrocatalytic reactions. Indeed, the ESSI analysis has also been applied to the ORR and correlations were found between $ESSI_{ORR}$ and $ESSI_{OER}$.[47] Recently, the two descriptors were used to simultaneously assess the OER and ORR activities of oxides in the search for bifunctional electrocatalysts.[24] In Figure 5 we present a combined plot for the ORR and the OER on a variety of oxides, including LSNMR ($La_{1.5}Sr_{0.5}NiMn_{0.5}Ru_{0.5}O_6$), a highly active double perovskite.

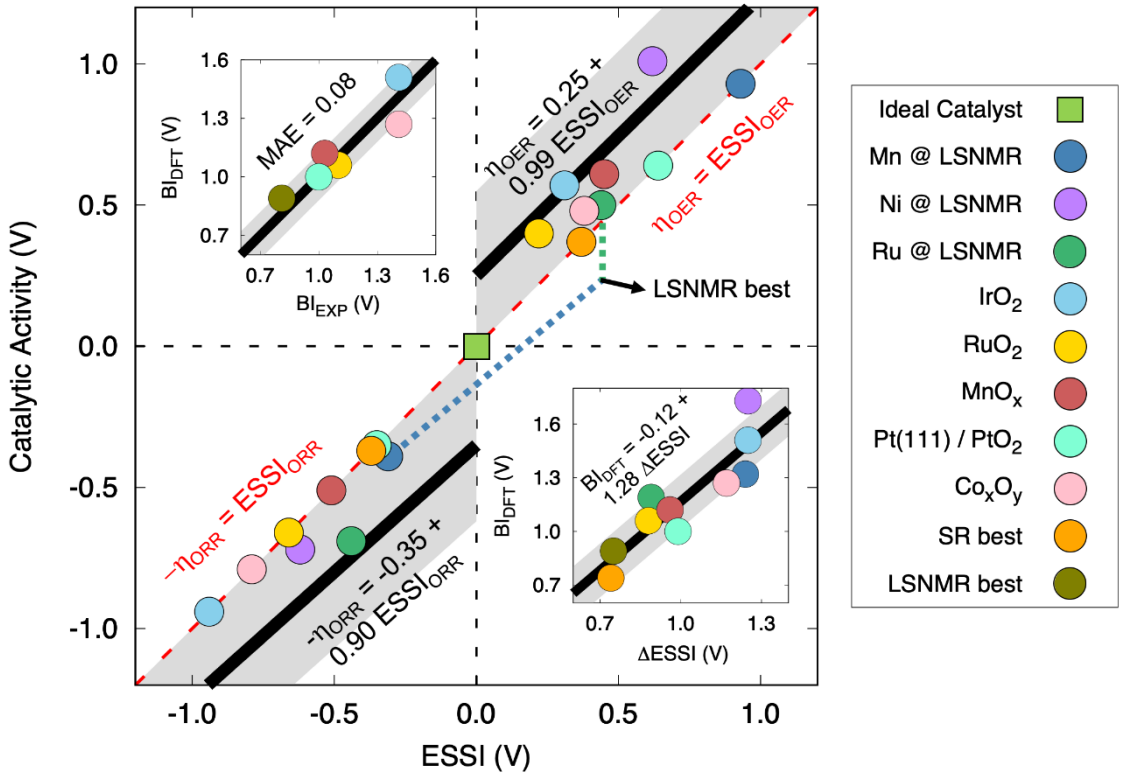

Figure 5. Calculated ORR and OER catalytic activities of selected oxides as a function of the electrochemical step symmetry index (ESSI). For the ORR, the catalytic activity is the additive inverse of the overpotential ($-\eta_{ORR}$). For the OER, the catalytic activity is the overpotential (η_{OER}). The bifunctional indices (BIs) of the materials are given by the vertical differences between the corresponding points (marked with blue/green dashed lines for LSNMR with ORR Mn sites and OER Ru sites, denoted LSNMR best). The black lines come from Figure 3 and the ORR data in the ESI. The gray area marks a confidence interval of 85%, located nearly ±0.3 eV around the blacklines. Bottom Inset: correlation between ΔESSI and BI. Top inset: Parity plot for experimental and DFT-calculated BIs. The MAE is only 0.08 V and is represented by the gray shaded stripe. This figure was redrawn with data from reference 24.

A simple metric for OER-ORR bifunctionality is the bifunctional index (*BI*),[48,49] which is defined as the positive difference between the potentials needed to achieve an OER current density of 10 mA/cm^2 and an ORR current density of −1 mA/cm^2. Following the analysis around Equations 1-8, the ideal ORR−OER bifunctional catalyst should have $BI \approx 0$ V . The analysis around Equations 9-10 suggests that an optimal catalyst obeying

scaling relations should have $BI \approx 1.60 - 0.86 \approx 0.74$ V (i.e. the difference between the two scaling-based limiting potentials). In practice, most catalysts display BIs larger than 1.0 V and those in the range 0.8-0.9 are regarded as highly bifunctional.[24,48,49]

Interestingly, the bottom inset in Figure 5 shows that the DFT-calculated BIs ($BI_{DFT} = \eta_{OER} + \eta_{ORR}$) are linearly correlated with the difference in ESSI ($\Delta ESSI = ESSI_{OER} - ESSI_{ORR}$). Furthermore, the top inset in Figure 5 shows that DFT-calculated BIs are generally in good agreement with the experimental ones. Therefore, the two insets establish a useful connection between ESSI and experimental bifunctionality.

Summary and conclusions

Rules of thumb are rather common and helpful in many branches of chemistry, physics, and engineering. Although they can greatly facilitate analyses and designs, it is important when resorting to them not to forget where they come from, as they probably resulted from analyses full of approximations and assumptions. Clearly, the ideal catalyst is not subject to scaling relations, but a compilation of data from the literature shows that the breaking of the OOH vs OH scaling relation does not per se lead to enhanced oxygen evolution electrocatalysis.

Instead, the electrochemical-step symmetry index (ESSI, which can be calculated irrespective of the presence or absence of adsorption-energy scaling relations between intermediates) and the δ–ε optimization are reasonable alternatives for the scaling-based and scaling-free design of enhanced electrocatalysts. The two alternatives suggest that catalytic enhancement may result more likely from focusing on specific steps rather than

on universal recipes. In sum, focusing on the actual potential-limiting steps seems a more advisable practice in electrocatalysis than using unverified rules of thumb.

Conflict of interest

The authors declare no conflicts of interest.

Acknowledgments

This work has been supported by Spanish MICIUN's RTI2018-095460-B-I00 and María de Maeztu MDM-2017-0767 grants and, in part, by Generalitat de Catalunya 2017SGR13, XRQTC grants and by COST Action 18234, supported by COST (European Cooperation in Science and Technology). F.C.V. thanks the Spanish MICIUN for a Ramón y Cajal research contract (RYC-2015-18996) and F.I. acknowledges additional support from the 2015 ICREA Academia Award for Excellence in University Research. O.P. thanks the Spanish MICIUN for an FPI PhD grant (PRE2018-083811). We are thankful to Red Española de Supercomputación (RES) for super-computing time at SCAYLE (projects QS-2019-3-0018, QS-2019-2-0023, and QCM-2019-1-0034). The use of supercomputing facilities at SURFsara was sponsored by NWO Physical Sciences.

References

1 N.-T. Suen, S.-F. Hung, Q. Quan, N. Zhang, Y.-J. Xu, and H. M. Chen, *Chem. Soc. Rev.*, 2017, **46**, 337-365.

2 T. Reier, H. N. Nong, D. Teschner, R. Schlögl, and P. Strasser, *Adv. Energy Mater.*, 2017, **7**, 1601275.

3 C. C. L. McCrory, S. Jung, J. C. Peters, and T. F. Jaramillo, *J. Am. Chem. Soc.*, 2013, **135**, 16977-16987.

4 Z. W. Seh, J. Kibsgaard, C. F. Dickens, I. Chorkendorff, J. K. Nørskov, and T. F. Jaramillo, *Science*, 2017, **355**, 146.

5 W. T. Hong, M. Risch, K. A. Stoerzinger, A. Grimaud, J. Suntivich, and Y. Shao-Horn, *Energy Environ. Sci*., 2015, **8**, 1404-1427.

6 X. Wang, J. Wang, and M. Sun, *Appl. Mater. Today*, 2019, **15**, 212-235.

7 F. E. Osterloh, *Chem. Soc. Rev.*, 2013, **42**, 2294-2320.

8 J. K. Nørskov, J. Rossmeisl, A. Logadottir, L. Lindqvist, J. R. Kitchin, T. Bligaard, and H. Jónsson, *J. Phys. Chem. B*, 2014, **108**, 17886-17892.

9 J. Rossmeisl, Z.-W. Qu, H. Zhu, G.-J. Kroes, and J. K. Nørskov, *J. Electroanal. Chem.* 2007, **607**, 83-89.

10 I. C. Man, H.-Y. Su, F. Calle-Vallejo, H. A. Hansen, J. I. Martínez, N. G. Inoglu, J. Kitchin, T. F. Jaramillo, J. K. Nørskov, and J. Rossmeisl, *ChemCatChem*, 2011, **3**, 1159-1165.

11 F. Abild-Pedersen, J. Greeley, F. Studt, J. Rossmeisl, T. R. Munter, P. G. Moses, E. Skúlason, T. Bligaard, and J. K. Nørskov, *Phys. Rev. Lett.*, 2007, **99**, 016105.

12 F. Calle-Vallejo, D. Loffreda, M. T. M. Koper, and P. Sautet, *Nat. Chem.*, 2015, **7**, 403-410.

13 M. M. Montemore, and J. W. Medlin, *Catal. Sci. Technol.*, 2014, **4**, 3748-3761.

14 J. Greeley, *Annu. Rev. Chem. Biomol. Eng*., 2016, **7**, 605-635.

15 B. Garlyyev, J. Fitchner, O. Piqué, O. Schneider, A. S. Bandarenka, and F. Calle-Vallejo, *Chem. Sci.*, 2019, **10**, 8060.

16 M. T. M. Koper, *J. Solid State Electrochem.*, 2013, **17**, 339-344.

17 M. García-Mota, A. Vojvodic, H. Metiu, I.C. Man, H.-Y. Su, J. Rossmeisl, and J. K. Nørskov, *ChemCatChem*, 2011, **3**, 1607–1611.

18 F. Calle-Vallejo, J. I. Martínez, and J. Rossmeisl, *Phys. Chem. Chem. Phys*., 2011, **13**, 15639-15643.

19 F. Calle-Vallejo, J. I. Martínez, J. M. García-Lastra, E. Abad, and M. T. M. Koper, *Surf. Sci*., 2013, **607**, 47-53.

20 F. Calle-Vallejo, A. Krabbe, and J. M. Garcia-Lastra, *Chem. Sci*., 2017, **8**, 124–130.

21 F. Calle-Vallejo, N. G. Inoglu, H.-Y. Su, J. I. Martínez, I. C. Man, M. T. M. Koper, J. R. Kitchin, and J. Rossmeisl, *Chem. Sci*., 2013, **4**, 1245–1249.

22 M. Retuerto, F. Calle-Vallejo, L. Pascual, P. Ferrer, A. García, J. Torrero, D. Gianolio, J. L. G. Fierro, M. A. Peña, J. A. Alonso, and S. Rojas, *J. Power Sources*, 2018, **404**, 56-63.

23 M. Retuerto, L. Pascual, F. Calle-Vallejo, P. Ferrer, D. Gianolio, A. G. Pereira, A. García, J. Torrero, M. T. Fernández-Díaz, P. Bencok, M. A. Peña, J. L. G. Fierro, and S. Rojas, *Nat. Commun*., 2019, **10**, 2041.

24 M. Retuerto, F. Calle-Vallejo, L. Pascual, G. Lumbeeck, M. T. Fernández-Díaz, M. Croft, J. Gopalakrishnan, M. A. Peña, J. Hadermann, M. Greenblatt, and S. Rojas, *ACS Appl. Mater. Interfaces*, 2019, **11**, 21454-21464.

25 F. Calle-Vallejo, O. A. Díaz-Morales, M. J. Kolb, and M. T. M. Koper, *ACS Catal*., 2015, **5**, 869-873.

26 G. A. Tritsaris, J. K. Nørskov, and J. Rossmeisl, *Electrochim. Acta*, 2011, **56**, 9783-9788.

27 E. M. Fernández, P. G. Moses, A. Toftelund, H. A. Hansen, J. I. Martínez, F. Abild-Pedersen, J. Kleis, B. Hinnemann, J. Rossmeisl, T. Bligaard, and J. K. Nørskov, *Angew. Chem. Int. Ed*., 2008, **47**, 4683-4686.

28 M. T. M. Koper, *J. Electroanal. Chem.*, 2011, **660**, 254-260.

29 M. Busch, N. B. Halck, U. I. Kramm, S. Siahrostami, P. Krtil, and J, Rossmeisl, *Nano Energy*, 2016, **29**, 126-135.

30 Z.-F. Huang, J. Song, S. Dou, X. Li, J. Wang, and X. Wang, *Matter*, 2019, **1**, 1494-1518.

31 J. Pérez-Ramírez, and N. López, *Nat. Catal.*, 2019, **2**, 971-976.

32 Y. Li, and Q. Sun, *Adv. Energy Mater*., 2016, **6**, 1600463.

33 A. A. Peterson, and J. K. Nørskov, *J. Phys. Chem. Lett.*, 2012, **3**, 251-258.

34 J. H. Montoya, C. Tsai, A. Vojvodic, J. K. Nørskov, *ChemSusChem*, 2015, **8**, 2180-2186.

35 R. R. Rao, M. J. Kolb, N. B. Halck, A. F. Pedersen, A. Mehta, H. You, K. A. Stoerzinger, Z. Feng, H. A. Hansen, H. Zhou, L. Giordano, J. Rossmeisl, T. Vegge, I. Chorkendorff, I. E. L. Stephens, and Y. Shao-Horn, *Energy Environ. Sci*., 2017, **10**, 2626-2637.

36 M. J. Craig, G. Coulter, E. Dolan, J. Soriano-López, E. Mates-Torres, W. Schmitt, and M. García-Melchor, *Nat. Commun*., 2019, **10**, 4993.

37 J. Hessels, R. J. Detz, M. T. M. Koper, J. N. H. Reek, *Chem. Eur. J*., 2017, **23**, 16413-16418.

38 F. Calle-Vallejo, and M. T. M. Koper, *ACS Catal.*, 2017, **7**, 7346-7351.

39 V. Tripkovic, *Phys. Chem. Chem. Phys*., 2017, **19**, 29381.

40 Z.-D. He, S. Hanselman, Y.-X. Chen, M. T. M. Koper, and F. Calle-Vallejo, *J. Phys. Chem. Lett.*, 2017, **8**, 2243-2246.

41 L. G. V. Briquet, M. Sarwar, J. Mugo, G. Jones, and F. Calle-Vallejo, *ChemCatChem*, 2017, **9**, 1261-1268.

42 K. S. Exner, and H. Over, *Acc. Chem. Res*., 2017, **50**, 1240-1247.

43 C. F. Dickens, C. Kirk, and J. K. Nørskov, *J. Phys. Chem. C*, 2019, **123**, 18960-18977.

44 K. S. Exner, *ACS Appl. Energy Mater*., 2019, **2**, 7991-8001.

45 K. S. Exner, and H. Over, *ACS Catal*., 2019, **9**, 6755-6765.

46 N. Govindarajan, M. T. M. Koper, E. J. Meijer, and F. Calle-Vallejo, *ACS Catal*., 2019, **9**, 4218-4225.

47 N. Govindarajan, J. M. García-Lastra, E. J. Meijer, and F. Calle-Vallejo, *Curr. Opin. Electrochem.*, 2018, **8**, 110-117.

48 J. Masa, W. Xia, I. Sinev, A. Zhao, Z. Sun, S. Grützke, P. Weide, M. Muhler, and W. Schuhmann, *Angew. Chem. Int. Ed.*, 2014, **53**, 8508-8512.

49 K. Elumeeva, J. Masa, F. Tietz, F. Yang, W. Xia, M. Muhler, and W. Schuhmann, *ChemElectroChem*, 2016, **3**, 138-143.